Separate-Structure UDE-Based Current Resonant Control Strategy on LCL-Type Grid-Tied Inverters With Weighted Average Current Method for Improved Injected Current Quality and Robustness

Yongkang Xiong, Yongqiang Ye, *Senior Member, IEEE*, Yongfeng Cao, and Yuheng Wu, *Student Member, IEEE*

***Abstract*—Due to its effective high-frequency suppression ability, the *LCL* filter has been widely used between inverters and the grid. However, its resonance causes system instability. The weighted-average current (WAC) strategy has been extensively studied to suppress resonance. By selecting a proper weight factor of the inductor and injected current, the order of the *LCL* can be reduced to first without resonance in the control loop, which can significantly simplify the controller design. Nevertheless, disturbances and uncertainties in the system will affect the control performance of the inverter. In this article, for a WAC-form *LCL* grid-tied inverter, a separate-structure uncertainty and disturbance estimator (SUDE) inner-loop control strategy with a zero-phase, low-pass, time-delay FIR filter is designed in the discrete domain to eliminate the influence of disturbances and parameter uncertainties on the system, and a proportional resonant controller is adopted as an outer-loop controller. By using the proposed FIR filter, the performance in the rejection of high-frequency harmonics is improved. Moreover, the stability of the proposed two-degree-of-freedom compound controller is analyzed in detail, and the superiority and effectiveness of its robustness to grid impedance and harmonic rejection are shown. Finally, the proposed strategies are validated on a 2-kW experimental platform.**

***Index Terms*—Grid-tied inverter, LCL filter, separate-structure uncertainty and disturbance estimator (SUDE), time-delay filter, weighted-average current (WAC) strategy.**

Manuscript received December 30, 2019; revised March 22, 2020; accepted May 1, 2020. Date of publication May 13, 2020; date of current version July 31, 2020. This work was supported in part by the National Natural Science Foundation of China under Grant 61973157, and in part by the Six Talent Peaks Program of Jiangsu Province under Grant 2016-XNY-030. Recommended for publication by Associate Editor M. Liserre. *(Corresponding author: Yongqiang Ye.)*

Yongkang Xiong was with the College of Automation Engineering, Nanjing University of Aeronautics and Astronautics, Nanjing 211106, China, He is now with the School of Information Engineering, Nanchang University, Nanchang 330031, China (e-mail: yongkang_xiong@foxmail.com).

Yongqiang Ye is with the College of Automation Engineering, Nanjing University of Aeronautics and Astronautics, Nanjing 211106, China, and also with the School of Electronic and Information, Zhongyuan University of Technology, Zhengzhou 450007, China. (e-mail: yongqiang_leaf@hotmail.com).

Yongfeng Cao and Yuheng Wu are with the College of Automation Engineering, Nanjing University of Aeronautics and Astronautics, Nanjing 211106, China. (e-mail: caoyongfeng@outlook.com; yuhengwu@email.uark.edu).

Color versions of one or more of the figures in this article are available online at http://ieeexplore.ieee.org.

Digital Object Identifier 10.1109/TPEL.2020.2994575

I. Introduction

A GRID-TIED inverter, an interface connecting distributed power generation system and a power grid, plays a vital role in ensuring that high-quality power is injected into the grid. Due to the harmonics caused by the pulsewidth modulation (PWM), a filter, of a type such as L, LCL, $LCCL$, or $LLCL$, needs to be adopted in grid-tied inverters. Among these, the L-type filter has a simple structure. The LCL filter can offer a relatively stronger filtering ability and allow the use of smaller inductors to meet harmonic limits, but it has a resonance, which may cause instability [1], [2]. To stabilize the system, many approaches have been proposed in the literature, e.g., passive damping (PD) methods [3] and active damping (AD) methods [2], [4]–[6]. Benefiting from their low cost, AD methods have become popular damping techniques in LCL-type grid-tied inverters.

According to their implementation, the types of AD methods can be divided into state feedback methods [2], [7], notch filter methods [8], state-space control methods [9], [10], etc. For the notch filter, the notch frequency is usually set to the resonant frequency of the LCL filter. Under nominal conditions, the resonance can be suppressed by the notch filter, and the system is stable. However, due to the variations and uncertainties of the system parameters, the suppression will be ineffective. For the state-feedback-type AD, two loops are introduced into the inverter, and then the system can be stabilized by designing a proper feedback gain. Based on modern control theory, the state-space control method with high robustness is proposed in [9]. Still, users needed to have high-level expertise to understand and implement it because a direct discrete-time pole-placement strategy and a Kalman filter were used in this article. The weighted-average current (WAC) strategy [11], a type of AD, can reduce the order of the controlled part of the LCL-type inverter from third to first by selecting an appropriate indirect current to trace the reference current, and there is no resonance in this control. The WAC strategy can be implemented by both hardware and software; the hardware approach is implemented by changing the structure of the circuit (i.e., $LCCL$), and the software approach is implemented by selecting the WAC of the injected current as well as the inductor current as the controlled

current [11]. Moreover, the whole inverter system with the WAC strategy consists of a controlled part and an uncontrolled part [12]–[16]. Resonance may still exist in the uncontrolled part even though the controlled part can be considered equivalent to a first-order resonance-free L filter for which it is easy to design a stable system.

To stabilize the whole inverter system, extra damping needs to be introduced into the inverter. With the help of the state feedback AD, an extra feedback loop was investigated in [15] and [16]. By designing a proper feedback gain, the AD-type WAC inverter can be stable and has satisfactory performance under nominal parameter conditions. However, the feedback gain needs to be carefully designed. Alternatively, as described in [12]–[14], only a slight PD resistance (the parasitic resistance of the filter capacitor) was required to achieve sufficient damping performance, which is very convenient in controller design. Both damping-type WAC strategies have been investigated and obtained satisfactory performance in the literature. In practice, however, due to the influence of system uncertainties and disturbances (e.g., the grid, unmodeled dynamics, dead time, and delays), the preset weight value designed according to the parameters of the ideal system will not be in line with the actual weight value, which will make the WAC system fail to reduce to first-order precisely, and the stability and control performance will be affected.

Different methods were proposed in recent works to improve the robustness and disturbance rejection performance of the WAC inverter. In [13], by selecting a proper weight coefficient of the WAC and considering the parasitic resistance, the system was robust to grid-impedance variation, and a proportional-resonant (PR) regulator was adopted to achieve a zero steady-state error in the injected current at the fundamental frequency. However, the PR regulator had difficulty rejecting disturbances other than the fundamental frequency disturbance [17]. In [12], unlike [13], a reference-model-tracking-type uncertainty and disturbance estimator (RUDE) based control strategy for $LCCL$ inverters was proposed. It combined the uncertainties and disturbances of the inverter into a total uncertainty and disturbance (TUD), which was estimated by the measurable state variables of the inverter. Then, a simple tuning method was proposed in [12]. The waveform quality of the injected current was insufficient, however, and a grid voltage full feedforward (GVFF) strategy was adopted in this method, which brought additional positive feedback of the grid current and might cause the system instability [18]. In addition, only the power grid, a known disturbance, can be compensated by the GVFF strategy[19], which fails in the case of other unknown disturbances. Therefore, the design of the uncertainty and disturbance estimator (UDE) based controller for the WAC LCL inverter with satisfactory disturbance rejection and robustness performance is important.

As investigated in [20] and [21], the combined disturbances of inverters include a series of harmonics. A time-delay low-pass filter form UDE can provide better disturbance rejection performance compared with the conventional low-pass filter form UDE. In [22], a RUDE-based control strategy was proposed for the LCL grid-tied inverter with capacitor-current-feedback AD. With the help of a time-delay filter, the injected current quality of the inverter has been improved. However, the design of the controller in [22] is slightly complicated because the parameters are coupled with each other. In the literature, a new type of UDE named the separate-structure uncertainty and disturbance estimator (SUDE) was proposed first in [20]. Although, under finite bandwidth, the reference model and the disturbance rejection function are coupled in both the RUDE [23] and SUDE , they can be designed separately in the SUDE. The SUDE has been applied to the constant voltage and constant frequency (CVCF) inverter [24], where a time-delay infinite impulse response (IIR) low-pass filter SUDE is employed in the voltage-loop control. Still, a phase lag is introduced by the low-pass filter. To compensate for the lag, an approximate compensation implemented easily within a low-frequency range was proposed.

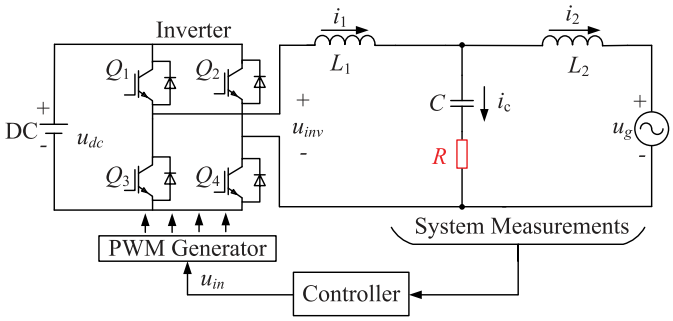

Fig. 1. System topology of a grid-tied inverter with an LCL filter.

In this article, compared with those SUDE-based control strategies with a conventional IIR low-pass filter designed in the s-domain, a modified SUDE-based control strategy for the WAC grid-tied inverter is proposed as an inner-loop, which employs a time-delay, FIR, zero-phase, low-pass filter to reject the periodic harmonics within the bandwidth of the filter and regulate the plant toward nominal conditions. Then, a properly designed PR controller is introduced in the outer loop. Moreover, the stability of the proposed compound controller is analyzed in detail. Due to the excellent disturbance rejection capabilities of the SUDE with the proposed FIR filter, the compound controller can provide better tracking performance compared with the PR controller and the PR with the GVFF controller. Furthermore, the robustness to grid impedance of the proposed compound controller is analyzed in theory and verified in experiments.

II. Modeling an LCL Filter With the WAC Strategy

Fig. 1 shows the topology of a single-phase grid-tied inverter with an LCL filter, where $u_{\rm dc}$, $u_{\rm inv}$, $u_{\rm in}$, u_g, L_1, L_2, C, and R are the dc bus voltage, the input voltage of the LCL filter, the controller output, the grid, the inverter-side inductor, the grid-side inductor, the filter capacitor, and the damping resistance, respectively. As proposed in [11], the weighted current of the inductor i_1 and the injected current i_2 is selected as the control current instead of i_2, which can be expressed as

$$i_w = \gamma i_1 + (1-\gamma) i_2 \tag{1}$$

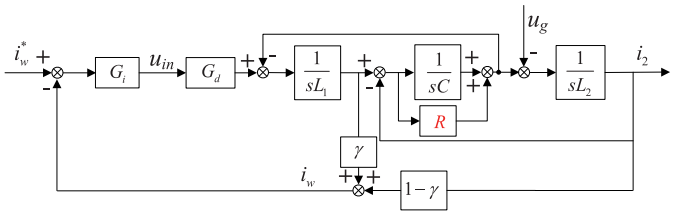

Fig. 2. Diagram of the WAC strategy for the grid-tied inverter with an LCL filter.

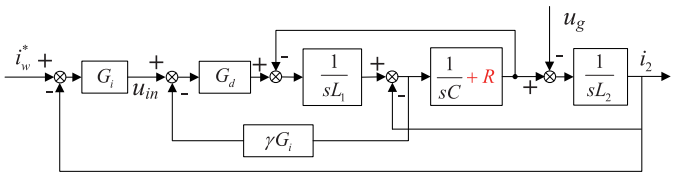

Fig. 3. Equivalent transformation of the block diagram of the WAC strategy system.

where i_w and γ are, respectively, the weighted current and the ratio of L_1 to the total inductance L (i.e., $L = L_1 + L_2$, $L_1 = \gamma L$). Referring to Fig. 1 and the idea of WAC, the diagram of the WAC strategy for the grid-tied inverter with an LCL filter can be obtained, as shown in Fig. 2, in which $G_i(s)$ is a feedback controller and $G_d(s)$ is the PWM gain k_{pwm} multiplied by one sampling period computation plus the half-sampling period PWM delays (i.e., $G_d(s) = k_{\text{pwm}} e^{-1.5T_s s}$, where T_s is the sampling period) [25].

According to Fig. 2, considering that $L_1 = \gamma(L_1 + L_2)$ and $L_2 = (1-\gamma)(L_1 + L_2)$, the transfer functions from u_{in} to i_w and i_2 can be expressed, respectively, as

$$\frac{i_w(s)}{u_{\text{in}}(s)} = \frac{\gamma s^2 L_2 C + sRC + 1}{s^3 L_1 L_2 C + s^2 RLC + sL} G_d(s) = \frac{G_d(s)}{(L_1 + L_2)s} \tag{2}$$

and

$$\frac{i_2(s)}{u_{\text{in}}(s)} = \frac{sRC + 1}{s^3 L_1 L_2 C + s^2 RLC + sL} G_d(s). \tag{3}$$

Then, by combining (2) and (3), we can obtain

$$\frac{i_2(s)}{i_w(s)} = \frac{i_2(s)}{u_{\text{in}}(s)} \cdot \frac{u_{\text{in}}(s)}{i_w(s)} = \frac{sRC + 1}{\gamma s^2 L_2 C + sRC + 1}. \tag{4}$$

To reveal the resonance suppression principle of the WAC strategy, an equivalent model will be built, where i_2 is the target control variable. According to Fig. 2 and combining (2)–(4), the equivalent open-loop transfer function $G_{\text{op\_}r}(s)$ with unit feedback from the reference current i_w^* to the injected current i_2 can be expressed in (5), as shown at the bottom of this page, and the corresponding diagram is shown in Fig. 3.

Fig. 3 suggests that there is an equivalent inherent capacitor-current-feedback damping (i.e., $\gamma G_i(s)$) in the WAC. Without the damping resistance (i.e., R), $G_{\text{op\_}r}(s) = -1$ will be established at the resonant frequency of LCL under the nominal parameter condition (i.e., $L_1 = \gamma(L_1 + L_2)$), which means that the system is critically stable and additional compensation is required. Furthermore, according to Fig. 2, it is notable that the whole system consists of a controlled part ($i_w(s)/u_{\text{in}}(s)$) and an uncontrolled part ($i_2(s)/i_w(s)$), which means that the stability of the whole system is determined by the stability of both the controlled and uncontrolled parts. According to (4), the uncontrollable part of the system is unstable when $R = 0$, which suggests that the whole system may be unstable, even if the closed-loop of the controllable part is stable. To stabilize the whole system, as described in Section I, a PD method with simple implementation can be adopted. Still, the uncertainties and disturbances of the system must be considered even when the PD is well designed, since the transfer functions of the system are not always true, as TUD will distort them. To improve the disturbance rejection and robustness performance of the WAC controlled inverter with PD, a SUDE-based resonant control strategy is proposed.

III. Current Control Strategy

A. Formation of SUDE-Based Current Controller With a Time-Delay Filter

According to (2), the voltage equation of the WAC LCL filter inverter with unity gain and delays can be derived as

$$L\frac{di_w(t)}{dt} = u_{\text{in}}(t - T_d) - u_g(t) \tag{6}$$

where $T_d = 1.5T_s$ and u_{in} is the controller output variable. Considering the disturbances and uncertainties of the inverter, the state equation of the inverter can be expressed as

$$\dot{i}_w(t) = \Delta a i_w(t) + (L^{-1} + \Delta b) u_{\text{in}}(t - T_d) + d(t) \tag{7}$$

where Δa and Δb are the unknown dynamic coefficients of the grid-tied inverter and $d(t)$ consists of the known (e.g., $-L^{-1}u_g(t)$) and unknown disturbances. In line with the conventional UDE [12], [26], [27], the TUD is unified into a combined disturbance. As in [24], the control signal u_{in} is split into a two-degree-of-freedom (2DOF) structure. Following the method mentioned above, the state function (7) can be rewritten as follows:

$$\dot{i}_w(t) = L^{-1}[u_t(t - T_d) - u_d(t - T_d) + f(t)] \tag{8}$$

where

$$\begin{cases} u_{\text{in}}(t - T_d) = u_t(t - T_d) - u_d(t - T_d) \\ f(t) = L[\Delta a i_w(t) + \Delta b u_{\text{in}}(t - T_d) + d(t)]. \end{cases} \tag{9}$$

In (9), $u_t(t)$, $u_d(t)$, and $f(t)$ represent the output of the tracking controller, the output of the disturbance and uncertainty estimator, and the TUD, respectively. To reject $f(t)$ in (8) and make the

$$G_{\text{op\_}r}(s) = \frac{i_2(s)}{i_w^*(s) - i_2(s)} = \frac{G_i(s)G_d(s)(1 + sRC)}{s^3 L_1 L_2 C + \gamma s^2 G_i(s) G_d(s) L_2 C + s^2 R(L_1 + L_2)C + s(L_1 + L_2)} \tag{5}$$

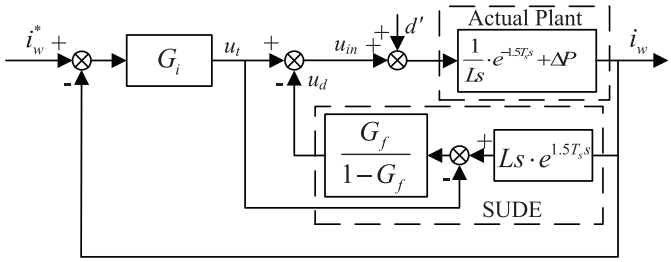

Fig. 4. Block diagram of the SUDE-based control system.

system TUD-free, according to the means in [20], an appropriate $u_d(t)$ should be designed here.

It is evident from (8) that $f(t)$ can be derived as

$$f(t) = L\dot{i}_w(t) - u_t(t - T_d) + u_d(t - T_d) \tag{10}$$

which means that the TUD $f(t)$ can theoretically be obtained from the derivative of $i_w(t)$ and the input of the plant. However, this cannot be directly used in the control law because $\dot{i}_w(t)$ is not causal and will amplify the measurement noise. Luckily, by introducing a filter, this problem can be circumvented. Following this idea, $f(t)$ can be estimated by being passed through a proper filter $g_f(t)$, i.e.,

$$f_e(t) = f(t) * g_f(t) \tag{11}$$

where $f_e(t)$ is the estimate of $f(t)$ and $*$ is the convolution operator. According to (8), the TUD will be approximately rejected if $u_d(t - T_d) \approx f_e(t)$, and the inverter system will approach the nominal system. The main idea of the SUDE in this article is to use the known variables to estimate the unknown ones and establish a corresponding compensation in the control to eliminate the influence of disturbances and uncertainties on the system. By combining (11) and (10), replacing $f_e(t)$ with $u_d(t - T_d)$, and taking the Laplace transform, we can obtain

$$\begin{aligned} u_d(s)e^{-1.5T_s s} = [&Lsi_w(s) - u_t(s)e^{-1.5T_s s} \\ &+ u_d(s)e^{-1.5T_s s}]G_f(s) \end{aligned} \tag{12}$$

and

$$u_d(s) = [Lsi_w(s)e^{1.5T_s s} - u_t(s)]\frac{G_f(s)}{1 - G_f(s)}. \tag{13}$$

Equation (13) indicates that with an appropriate $G_f(s)$, the system states (i_w) and tracking controller output (u_t) can be utilized to obtain the estimate of the TUD (u_d).

Fig. 4 shows the block diagram of the SUDE-based control system, where $G_i(s)$ is the controller, the actual plant consists of the nominal plant $e^{-1.5T_s s}1/Ls$ and the unmodeled dynamics $\Delta P(s)$, and $d'(s)$ is the disturbance coupled with the unmodeled system, which can be derived from (7) (cf. Appendix) and expressed as

$$\begin{cases} \Delta P(s) = \left[\dfrac{1}{s - \Delta a}\left(\dfrac{1}{L} + \Delta b\right) - \dfrac{1}{Ls}\right] e^{-1.5T_s s} \\ d'(s) = \dfrac{Ls}{(s - \Delta a)(e^{-1.5T_s s} + Ls \cdot \Delta P(s))} d(s). \end{cases} \tag{14}$$

As illustrated in Fig. 4, the SUDE can be easily implemented to estimate the TUD after a suitable $G_f(s)$ is selected. Thus, the design of the SUDE controller is converted to the design of the filter $G_f(s)$.

We can replace $u_d(t - T_d)$ with $f_e(t)$ in (8) and substitute (11) into it; with the Laplace transform taken, we can obtain

$$si_w(s) = L^{-1}\left[u_t(s)e^{-1.5T_s s} + (1 - G_f(s))\, f(s)\right]. \tag{15}$$

Clearly, $f(s)$ can be rejected in the case of 1-$G_f(s)$=0. Hence, the SUDE-based control allows decoupling of the reference tracking design and disturbance rejection design, which shows that the SUDE has a 2DOF nature within the bandwidth of $G_f(s)$.

In general, $G_f(s)$ can be chosen as a low-pass filter, but it is not an optimal choice in this article because, according to the characteristics of inverters, the harmonic rejection performance will be significantly improved by choosing the time-delay filter [24]. Furthermore, due to the causality issue caused by $e^{1.5T_s s}$, the SUDE (13) cannot be directly implemented by adopting a conventional low-pass filter. Referring to [24], the time-delay filter can be used, which is expressed as

$$G_f(s) = e^{-T_p s}G_c(s) \tag{16}$$

where T_p is the period of the fundamental signal (i.e., 0.02 s in this article), and $G_c(s)$ is a conventional third-order IIR filter.

$G_c(s)$ will introduce a nonlinear phase lag, which will affect the control performance [24]. To compensate for the phase lag, an available approach implemented by reducing the delay (T_p) was proposed in [24], and the compensated $G_f(s)$ can be expressed as $G_{f\_c}(s)$. However, that compensation method is approximate, because reducing the delay time can be regarded as introducing a linear lead compensation, through which the influence of phase lag can be eliminated approximately in a certain frequency range, but the elimination is invalid at high frequencies (a similar claim can be found in [24], which will not be discussed here). Thus, a FIR zero-phase and time-delay filter $\tilde{G}_f(z)$ is adopted instead of $G_{f\_c}(s)$, considering the discrete-time implementation, and $\tilde{G}_f(z)$ can be expressed as

$$\tilde{G}_f(z) = z^{-200}G_{\text{low}}(z) \tag{17}$$

where $G_{\text{low}}(z)$ is a zero-phase low-pass filter, which can be expressed as

$$G_{\text{low}}(z) = h(0) + \sum_{1}^{n} h(k)(z^k + z^{-k}) \tag{18}$$

where n is half of the order of $G_{\text{low}}(z)$, and $h(k)$ are the coefficients of the filter. Since z^{-200} exists in (17), $\tilde{G}_f(z)$ is realizable even though $G_{\text{low}}(z)$ itself is noncausal. Moreover, (13) is also realizable with $z^{1.5}$ ($e^{1.5T_s s}$) approximated by $z(0.5 + 0.5z)$.

To compare the disturbance rejection performance with different filters, the expressions of $G_c(s)$, $G_{f\_c}(s)$, and $\tilde{G}_f(z)$ are listed in Table I, where their low-pass filter bandwidth is set to 500 Hz, $\omega_F = 1000\pi$ rad/s, and the zero-phase low-pass filter $G_{\text{low}}(z)$ is a 20th-order FIR filter whose coefficients are obtained by executing the MATLAB function "fir1" and are expressed in Table II.

Fig. 5 shows the disturbance rejection performance with different filters, which suggests that compared with $1 - G_c(s)$, $1 - G_{f\_c}(s)$ and $1 - \tilde{G}_f(z)$ can introduce a stronger rejection

TABLE I
EXPRESSIONS OF FILTERS

Filter	Expression
G_c	$\dfrac{\omega_F^3}{s^3+2\omega_F s^2+2\omega_F^2 s+\omega_F^3}$
G_{f_c}	$G_c e^{\{-0.02+\frac{1}{100\pi}\arctan[\frac{200\pi\omega_F^2-(100\pi)^3}{\omega_F^3-2(100\pi)^2\omega_F}]\}s}$
$\tilde{G}_f$	$\left[h(0)+\sum_1^{10}h(k)(z^k+z^{-k})\right]z^{-200}$

TABLE II
COEFFICIENTS OF $G_{\text{low}}(z)$

k	0	1	2	3	4	5
$h(k)$	0.1185	0.1139	0.1011	0.0824	0.06116	0.04072
k	6	7	8	9	10	
$h(k)$	0.02378	0.01175	0.00465	0.001327	3.694e-19	

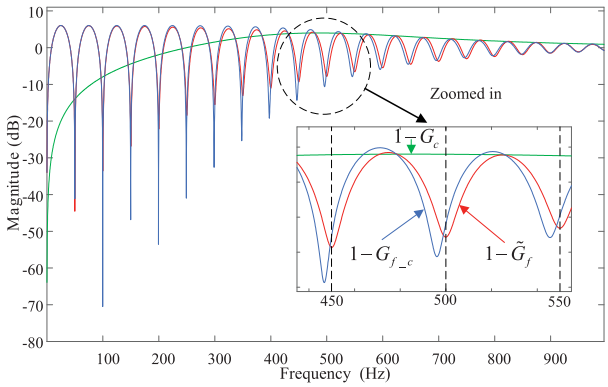

Fig. 5. Bode diagrams of disturbance rejection performance with different filters but the same low-pass filter bandwidth.

at resonant frequencies. Furthermore, the notch frequency of $1-\tilde{G}_f(z)$ is accurate, as desired. The notch frequency of $1-G_{f\_c}(s)$, however, shifts within the high-frequency range of the bandwidth even though the computational burden of using $\tilde{G}_f$ is heavier than that of using G_{f_c}. Thus, it is more reasonable to choose $\tilde{G}_f(z)$ as the filter used in the proposed SUDE. Moreover, according to Fig. 4, the design of the control system includes not only the design of the inner SUDE but also the outer feedback controller.

B. PR Controller Design

With the proper SUDE adopted, $f(t)$ can be largely cancelled by $u_d(t)$, and the actual system is approximated as a nominal system. For the nominal system, several strategies exist. Referring to [28], a PR controller is employed in this article, which is

$$G_i(s)=K_p+\frac{2K_r\omega_i s}{s^2+2\omega_i s+\omega_o^2} \tag{19}$$

where $\omega_o=2\pi f_o$ is the fundamental angular frequency, ω_i is the resonant cutoff frequency, which is the bandwidth of the resonant part, and a typical value of ω_i is π rad/s (i.e., there is a 1% variation of $2\pi f_o$) [29]. According to [28], the crossover frequency (ω_c) of the controlled system should be set first before calculating K_p and K_r. Moreover, at ω_c, $G_i(j\omega_c)$ can

TABLE III
EXPERIMENT PARAMETERS

Parameter	Value	Parameter	Value
DC bus voltage u_{dc}	380 V	PCC voltage u_{PCC}	220 V
PWM frequency f_c	10 kHz	Sampling period T_s	100 μs
Inverter-side inductor L_1	3.8 mH	Grid-side inductor L_2	2.5 mH
Capacitor C_1	10 μF	Resistance R	4 Ω

be approximated as

$$G_i(j\omega_c)\approx K_p+\frac{2\pi K_r}{j\omega_c}. \tag{20}$$

Then, the phase angle of this forward-path loop gain at ω_c is given by

$$\begin{aligned}\angle\left(G_i(j\omega_c)P_0(j\omega_c)\right)&=\angle\left[\left(K_p+\frac{2\pi K_r}{j\omega_c}\right)\frac{1}{j\omega_c L}e^{-1.5j\omega_c T_s}\right]\\&=\arctan\left(\frac{K_p\omega_c}{2\pi K_r}\right)-\frac{\pi}{2}-\frac{\pi}{2}-1.5\omega_c T_s\\&=\phi_m-\pi\end{aligned} \tag{21}$$

where $P_0(s)=e^{-1.5T_s s}1/Ls$ is the nominal plant, and ϕ_m is the phase margin (PM). The parameters in Table III are used in the following design. According to (21), we can easily obtain

$$\phi_m=\arctan\left(\frac{K_p\omega_c}{2\pi K_r}\right)-1.5\omega_c T_s \tag{22}$$

and for a given ϕ_m, the maximum ω_c can be obtained in the case of $\arctan(K_p\omega_c/2\pi K_r)=\pi/2$; thus

$$\omega_{c\max}=\frac{\frac{\pi}{2}-\phi_m}{1.5T_s}. \tag{23}$$

By substituting $T_s=100$ μs and PM $=60^\circ$ into (23), we can calculate that $\omega_{c\max}$ is 3488 rad/s (500 Hz). In addition, referring to [30], ω_c can be chosen as 4% of ω_s $(2\pi/T_s)$, i.e., 2512 rad/s (400 Hz). To summarize, we choose $\omega_{\text{copt}}=$ 2600 rad/s. Recalling (23), the condition for its establishment is that $K_p\omega_{\text{copt}}/(2\pi K_r)>10$ exists, which means that $G_i(j\omega_c)$ in (19) can be further approximated as K_p. For a fixed ω_c, the relationship between P_0 and G_i is

$$|G_i(j\omega_c)P_0(j\omega_c)|=K_p\frac{1}{L\omega_c}=1. \tag{24}$$

By substituting ω_{copt} =2600 rad/s and $L=6.3$ mH into (24), then combining $K_p\omega_{\text{copt}}/2\pi K_r>10$, we can obtain $K_p=16.4$ and the maximum of K_r (i.e., $K_{r\max}$) $=678$. Then, recalling Fig. 4 and the nominal plant $P_0(z)$, we can obtain the closed-loop transfer function $G_{\text{cl}}(z)$ from $i_w^*(z)$ to $i_w(z)$ under the nominal model condition:

$$G_{\text{cl}}(z)=\frac{i_w(z)}{i_w^*(z)}=\frac{G_i(z)P_0(z)}{1+G_i(z)P_0(z)}. \tag{25}$$

IV. STABILITY STUDY

A. Stability Analysis of the Proposed System

The influence of system uncertainties and disturbances on system stability cannot be neglected, even when the controller parameters have been well designed. Specifically, as described

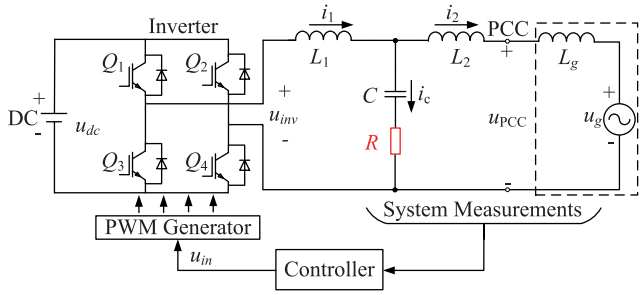

Fig. 6. System topology of the LCL inverter under weak grid conditions.

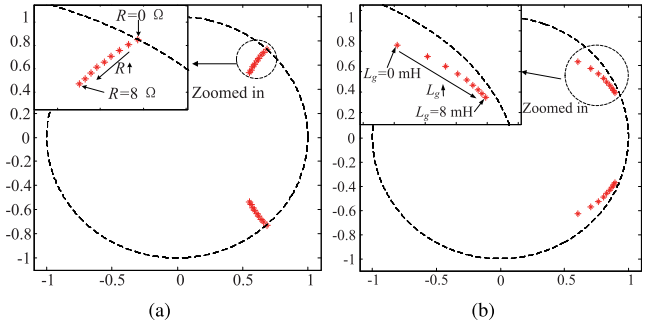

Fig. 7. Poles of the uncontrolled part. (a) With different R. (b) With different L_g.

in [31] and [32], the power grid is not an ideal voltage source but a voltage source and an impedance series structure (i.e., weak grid conditions). Fig. 6 shows the system topology of the LCL inverter under weak grid conditions. As shown, there is an inductor between the point of common coupling (PCC) and the grid. In this section, the robustness of the proposed strategy will be studied; the parameters of the inverter are listed in Table III.

1) Stability Analysis of the Uncontrolled Part: As described in Section II, the uncontrolled part affects the stability of the whole system. By substituting the parameters in Table III into (4) and performing a discrete transformation, we can have the poles of the uncontrolled part $i_2(z)/i_w(z)$ for different R and L_g values, where L_g is emulated by increasing L_2. Fig. 7(a) suggests that when $L_g = 0$, the poles move closer to the center of the unit circle with the increase of R. In particular, when R equals 0, the poles are on the unit circle, which is consistent with the analysis in Section II. As shown in Fig. 7(b), when R is selected as 4 Ω, the stability of $i_2(z)/i_w(z)$ can be guaranteed as L_g changes from 0 to 8 mH.

2) Stability Analysis of the Controlled Part: To study the influence of system uncertainties on the stability of the controlled part, considering L_g and omitting $d'(s)$, the modified block diagram of Fig. 4 is given in Fig. 8, where $P(z)$ is the actual plant. Additionally, the partial implementation of the SUDE ($z^{1.5}\tilde{G}_f(z)/[1-\tilde{G}_f(z)]$) in Fig. 8 is given in Fig. 9. Similarly, $\tilde{G}_f(z)/[1-\tilde{G}_f(z)]$ can be implemented similarly to $z^{1.5}\tilde{G}_f(z)/[1-\tilde{G}_f(z)]$, which is omitted here.

Recalling Fig. 2, with the weight factor unmatched (i.e., $\gamma \neq L_1/L$), $P(z)$ can be expressed as

$$P(z) = \frac{i_w(z)}{u_{\text{in}}(z)} = \mathcal{Z}\left(\frac{\gamma s^2 L_2 C + sRC + 1}{s^3 L_1 L_2 C + s^2 RLC + sL}\right) G_d(z) \tag{26}$$

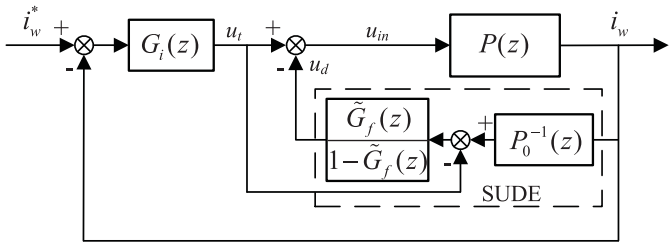

Fig. 8. Block diagram of the proposed SUDE-based control system.

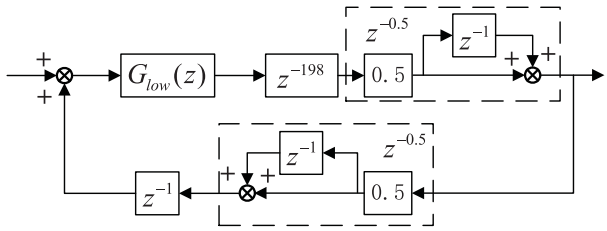

Fig. 9. Partial implementation diagram of the SUDE.

and thus, the closed-loop transfer function $\tilde{G}_{cl}(z)$ of Fig. 8 can be expressed as

$$\tilde{G}_{\text{cl}}(z) = \frac{G_i(z)P(z)}{1-\tilde{G}_f(z)+\dfrac{\tilde{G}_f(z)P(z)}{P_0(z)}+G_i(z)P(z)}. \tag{27}$$

Comparing (25) and (27), we find that the numerators in them are similar, but their denominators are different. We can rewrite the denominator in (27) as follows:

$$\begin{aligned} 1-\tilde{G}_f(z)+\frac{\tilde{G}_f(z)P(z)}{P_0(z)}+G_i(z)P(z) \\ = [1+G_i(z)P_0(z)][1+X(z)] \end{aligned} \tag{28}$$

where

$$X(z) = \frac{G_i(z)P(z)-G_i(z)P_0(z)-\tilde{G}_f(z)+\dfrac{P(z)\tilde{G}_f(z)}{P_0(z)}}{1+G_i(z)P_0(z)}. \tag{29}$$

Clearly, according to the small-gain theorem, the sufficient conditions for system stability can be obtained as follows:

1) $\dfrac{G_i(z)P(z)}{1+G_i(z)P_0(z)}$ is stable;
2) $\|X(z)\|_\infty < 1, \forall z = e^{j\omega}, 0 < \omega < \dfrac{\pi}{T_s}$.

Condition 1) is determined only by $P(z)$ when $G_i(z)$ and $P_0(z)$ are designed and selected well. The change in L_g is chosen to represent the uncertainty of $P(z)$ here. By substituting the proposed discrete PR controller $G_i(z)$ and $P_0(z)$ into condition 1), we can have the trend of condition 1) under varying R and L_g.

Fig. 10 shows the pole map of condition 1), where Fig. 10(a) shows the poles changing with R when L_g=2 mH and Fig. 10(b) shows the poles changing with L_2 when $R = 4\,\Omega$. It can be seen from Fig. 10(a) that the poles of condition 1) move closer to the center of the unit circle with the increase of R, and the damping resistance R required for condition 1) to move from

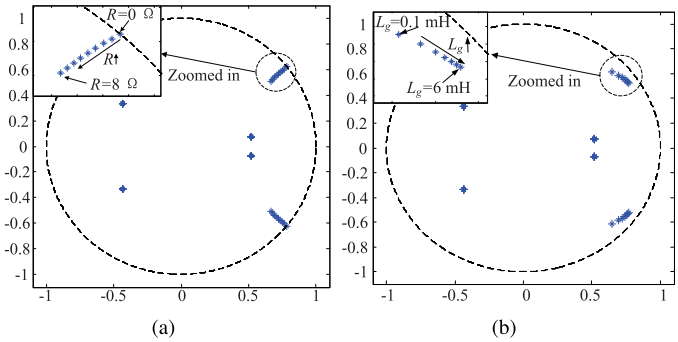

Fig. 10. Poles of condition 1). (a) With the variation of R. (b) With the variation of L_g.

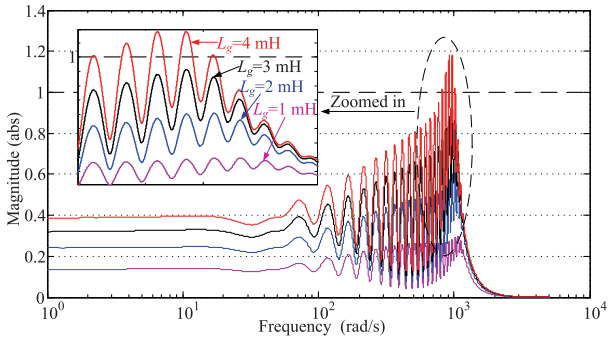

Fig. 11. Stability performance of the proposed control strategy with the variation of L_g.

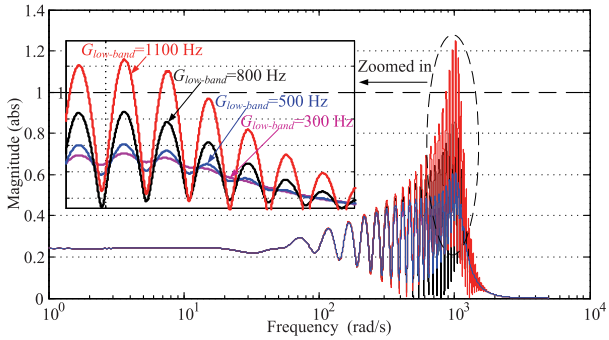

Fig. 12. Stability performance of the proposed control strategy with the variation of the low-pass filter bandwidth.

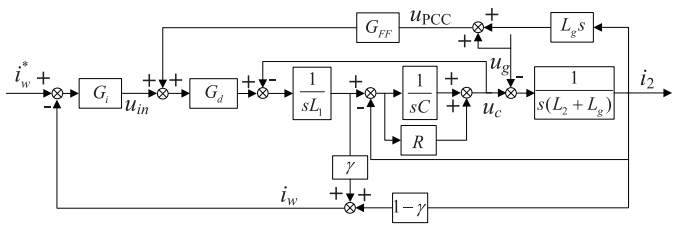

Fig. 13. Block diagram of the GVFF strategy for the WAC-form LCL inverter under weak grid conditions.

critical stability to stability is also small. Fig. 10(b) suggests that when $R = 4\ \Omega$, condition 1) can be satisfied with the increase of L_2 from 0 to 3 mH. Moreover, by substituting $G_i(z)$ and the filter $\tilde{G}_f(z)$ (where the bandwidth of G_{low} is 500 Hz) into $X(z)$, condition 2) with L_g changing from 0.1 to 4 mH is investigated.

As shown in Fig. 11, the x-axis represents the frequency, and the y-axis represents the magnitude of X, which is less than 1 with $L_g \leq 3$ mH. By combining Figs. 7, 10, and 11, we can conclude that the system stability can be guaranteed when $L_g \leq 3$ mH.

Furthermore, as indicated in Section III-A, the bandwidth of the low-pass filter G_{low} determines the range of disturbances and parameter uncertainties that can be rejected. The bandwidth of G_{low} should also be studied carefully, so we choose $L_g = 2$ mH to study the effect of the bandwidth of the low-pass filter on the stability of the proposed strategy. As shown in Fig. 12, the magnitude of $X(z)$ is less than 1 when the bandwidth of the low-pass filters is in the range from 300 to 800 Hz. For a sufficient stability margin, the bandwidth is set to 500 Hz.

B. Comparison With the GVFF Strategy

The aim of the SUDE strategy is to estimate and reject the TUD in the inverter. As a well-known external disturbance, the grid can be compensated by the GVFF strategy [19]. As described in Section I, however, the GVFF will affect the stability of the system under weak grid conditions. Furthermore, compared with the GVFF, the proposed SUDE is designed to reject other disturbances and system uncertainties in addition to the grid voltage. To demonstrate the differences between the two controls, a comparison between them is given.

1) Derivation and Analysis of the GVFF Strategy: To eliminate the effect of the grid voltage (i.e., u_g) on the injected current (i.e., i_2), the block diagram of the GVFF strategy for the WAC-form LCL inverter is given in Fig. 13, where G_{FF} is the transfer function of the GVFF. According to [19], G_{FF} can be derived as

$$G_{\text{FF}}(s) = 1 + \frac{\gamma Cs}{RCs+1} G_i(s) + \frac{CL_1 s^2}{RCs+1}. \tag{30}$$

Based on Fig. 13, we can obtain the transfer function from u_{in} to i_w, which can be expressed as (31) shown at the bottom of the next page. Compared with (26), a term related to G_{FF} (i.e., $(RCs+1)G_{\text{FF}}(s)G_d(s)L_g s$) is added in the denominator of (31).

2) Stability Performance of the GVFF and the SUDE Under Weak Grid Conditions: It is worth noting that the uncontrolled part of the system is not affected by the GVFF, and its expression is still (4); thus, only the controlled part of the system needs to be discussed here. According to the stability criteria proposed in Section IV-A, we can obtain the stability performance. For the GVFF, we can replace P in conditions 1) and 2) with G_{op} (31) and let $\tilde{G}_f$=0.

Fig. 14 shows the poles of stability condition 1) using the proposed SUDE and the GVFF with $R = 4\ \Omega$, which suggests that with the proposed SUDE, stability condition 1) is established when L_g is in the range 0–5 mH. However, with G_{FF} introduced, stability condition 1) is false when L_g >2 mH. Moreover, the result of stability condition 2) for the system with G_{FF} is given in Fig. 15. As indicated in Fig. 15, the magnitude of X becomes larger than 1 between $L_g = 1$ mH and 2 mH. By combining

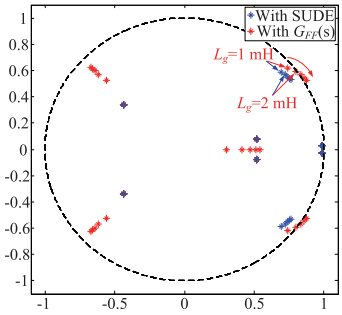

Fig. 14. Poles of condition 1) with the GVFF and the SUDE for different L_g.

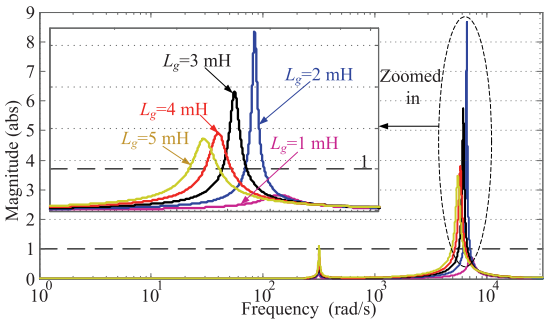

Fig. 15. Stability condition 2) with varying L_g.

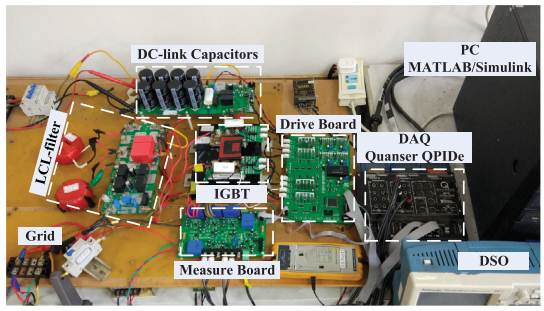

Fig. 16. Experimental setup.

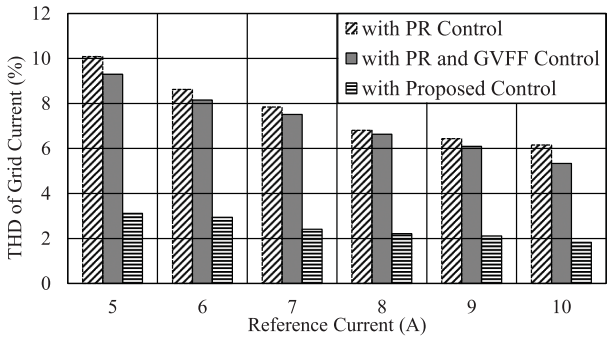

Fig. 17. THDs of the injected grid current with different i_w^*.

Figs. 14 and 15, we can conclude that with $G_{\rm FF}$ introduced, the system stability cannot be guaranteed when $L_g \geq 2$ mH.

Comparing the results of the SUDE and the GVFF [Figs. 10(b), 11, 14, and 15], we find that the proposed compound control can adapt to a broader range of the grid-impedance variation than the PR with GVFF control, although the stabilities of both strategies are affected by the grid-impedance change.

V. Experimental Verification

A. Setup

A 2-kW prototype of Fig. 1 is built to validate the effectiveness of the proposed scheme. The inverter consists of an insulated-gate bipolar transistor (IGBT) inverter bridge, an LCL filter, two voltage sensors for $u_{\rm PCC}$ used in the phase-locked loop and $u_{\rm dc}$, and two current sensors for i_1 and i_2. It is noteworthy that compared with the state-feedback form AD method, the proposed WAC strategy has the advantage of simplifying the controller design by reducing the order of the system. The resistance used in the proposed strategies is small, although both strategy require two current sensors. The single-phase grid-tied inverter is controlled by a Quanser QPIDe card, which is connected with a PC running MATLAB/Simulink and QuaRC. The experimental setup is shown in Fig. 16.

B. Experimental Results

Recalling the detailed design in Section III, we will summarize the parameters of the PR controller (K_p and K_r) and low-pass bandwidth as 16.4, 678, and 500 Hz here. Similar to the SUDE, the GVFF can also be considered as the compensator for the PR controller, so the control performance of the PR, the PR with GVFF, and the PR with SUDE will be studied. Note that the K_p and K_r in the three kinds of control are the same, and $G_{\rm FF}(s)$ is given in (30).

1) Steady-State Performance: To verify the antidisturbance performance of the proposed strategy, three sets of contrastive experiments under the nominal parameter but different power level conditions are performed.

As shown in Fig. 17, the x-axis represents the injected current levels, and the y-axis represents the total harmonic distortion (THD) of the injected current. Clearly, with the GVFF and SUDE introduced, the THDs of the injected current decrease in all power levels compared with the PR control strategy, especially when the power level is low, and the decrease with the SUDE is significant. The contrastive results of the three control methods under a 10 A reference current are given in Figs. 18–20, where e(rms) is the root-mean-square (rms) value of the error between the reference current and the injected current.

As shown in Figs. 18-20, the differences of the performance among the PR control, the PR with GVFF control, and the PR with SUDE under the nominal parameter condition are more

$$G_{\rm op}(s) = \frac{i_w(s)}{u_{\rm in}(s)} = \frac{\gamma s^2(L_2+L_g)C + RCs + 1}{s^3 L_1(L_2+L_g)C + (RCs+1)(L_1+L_2+L_g)s - (RCs+1)G_{\rm FF}(s)G_d(s)L_g s} G_d(s). \quad (31)$$

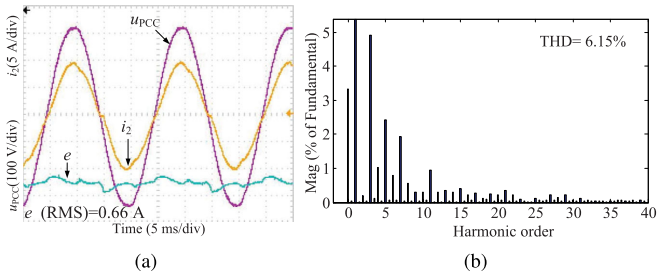

Fig. 18. Result of PR control. (a) Injected grid current i_2. (b) Spectrum of the injected grid current.

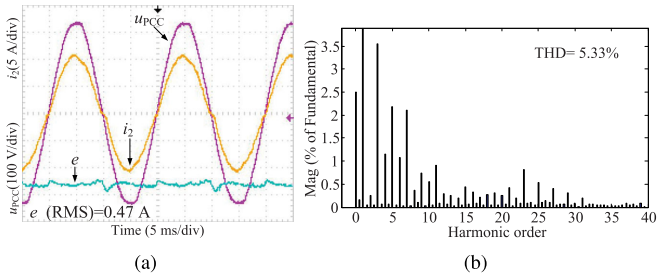

Fig. 19. Result of PR with GVFF control. (a) Injected grid current i_2. (b) Spectrum of the injected grid current.

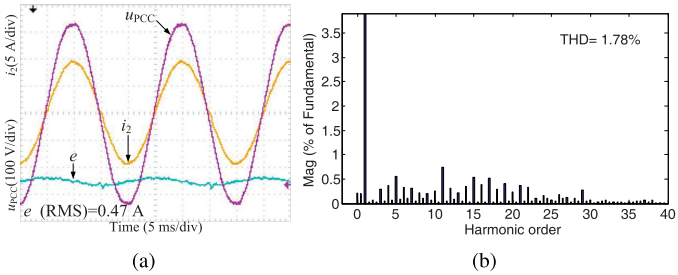

Fig. 20. Result of the proposed control. (a) Injected grid current i_2. (b) Spectrum of the injected grid current.

obvious. By combining Figs. 17–20, we can conclude that both the GVFF and the SUDE controls can improve the control performance of the system (including the tracking error and THD), and compared with the PR with GVFF control, the control performance of the proposed compound control is better.

2) Robustness Performance: Furthermore, in addition to controlling of the injected current quality, the robustness of the system is also worth studying. Without loss of generality, the experiments with L changing in the SUDE [i.e., (13)] have been chosen to verify the parameters' robustness of the proposed control strategy. According to (6) and (13), L is the total inductance of control, and a change in L can be regarded as a change in the actual physical inductor.

As shown in Fig. 21, the THD curves of the proposed control method are flat within the range from 79% to 119% (5 to 7.5 mH), and the level of the curve is low, which suggests that the proposed controller can remain stable in a certain range of parameter uncertainty. Furthermore, to study the robustness for the proposed control strategy to the variation of the impedance of the grid, experimental studies are performed here. An external inductor L_g is added between the PCC and the grid side.

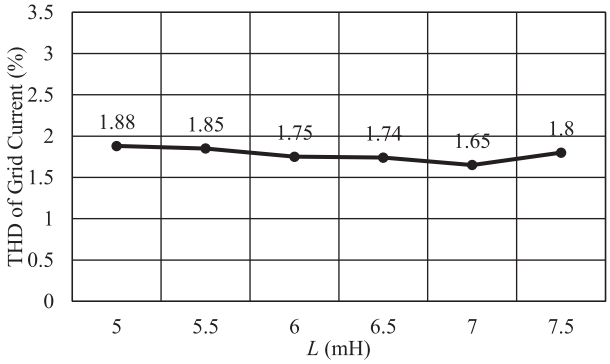

Fig. 21. THDs of the injected grid current with the variation of L.

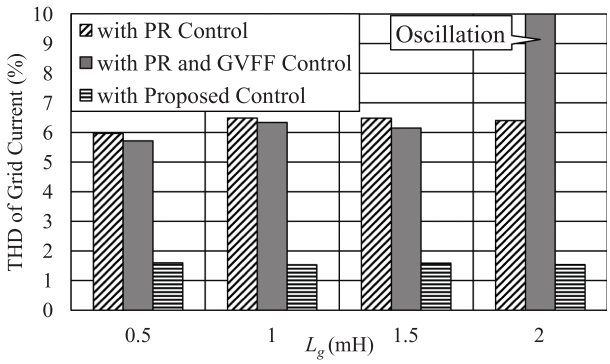

Fig. 22. THDs of the injected grid current with the variation of added L_g.

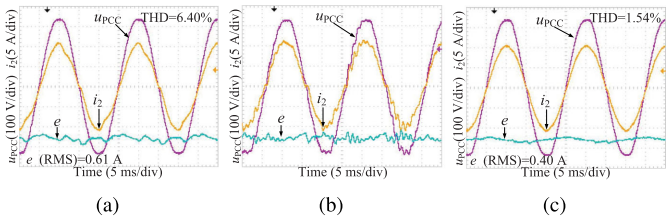

Fig. 23. Results of the PR, the PR with GVFF, and the PR with SUDE control in the case of L_g=2 mH. (a) PR control. (b) PR with GVFF control. (c) PR with SUDE control.

As indicated in Fig. 22, the PR and the proposed strategy are robust to the change of the added L_g from 0.5 to 2 mH, and the THDs of the injected current with the PR are larger than those with the proposed strategy. There is an oscillation in the injected current with the GVFF introduced when L_g=2 mH, although it is robust to L_g in the range of 0.5–1.5 mH. Specifically, the steady-state responses of the PR, the PR with GVFF, and the PR with SUDE for L_g=2 mH and i_w^*=10 A are given in Fig. 23. The stability performance of both the PR controller and the PR+SUDE compound controller is satisfactory. However, the injected current is distorted with the GVFF introduced. Thus, based on Figs. 22 and 23, we can conclude that the proposed compound control can adapt to a broader range of grid-impedance variation than GVFF, which is consistent with the conclusion of Section IV-B2.

3) Dynamic Performance: Fig. 24 shows the dynamic performance of the PR, the PR with GVFF, and the PR with the SUDE controller under the nominal parameter condition, where

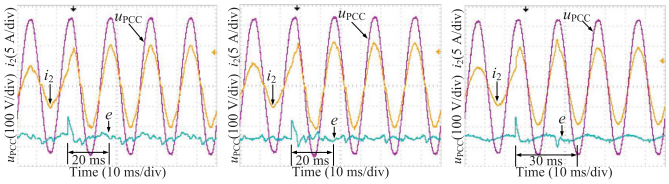

Fig. 24. Dynamic responses of the PR, the PR with GVFF, and the PR with SUDE control. (a) PR control. (b) PR with GVFF control. (c) PR with SUDE control.

the reference current steps from 5 to 10 A. The figure suggests that although the settling time of the system with the compound controller is slightly longer than that of the PR controller and the PR with the GVFF controller, the tracking performance of the compound controller is better.

VI. Conclusion

To suppress the resonance in the LCL grid-tied inverter, the WAC-strategy, an AD method, has attracted much attention due to its reduced-order characteristics. However, the antidisturbance ability of WAC falls short. In this article, considering 1.5 sampling period delays, a 2DOF compound controller composed of a PR controller and a SUDE with a zero-phase, low-pass, time-delay FIR filter is built to eliminate the influence of disturbances and uncertainties on the grid-tied inverter with a WAC and PD strategy. With the help of the SUDE with an FIR filter, the controlled part of the WAC-strategy LCL inverter system can remain first-order, and then the design of the PR controller becomes simpler. Compared with the conventional PR controller and the PR with the GVFF controller, the proposed controller shows its superiority and effectiveness in disturbance rejection, and the quality of the injected current is improved a lot. Moreover, the robustness of the proposed control to grid impedance has been analyzed. The effectiveness of the proposed strategy was verified on a 2-kW single-phase grid-tied inverter.

Appendix
The Derivation of (14)

By taking the Laplace transform, the state equation of (7) in the s-domain can be obtained as

$$si_w(s) = \Delta a i_w(s) + (L^{-1} + \Delta b)u_{\text{in}}(s)e^{-1.5T_s s} + d(s). \tag{A1}$$

$i_w(s)$ can be derived as

$$i_w(s) = \frac{(L^{-1} + \Delta b)u_{\text{in}}(s)e^{-1.5T_s s}}{s - \Delta a} + \frac{d(s)}{s - \Delta a} \tag{A2}$$

and

$$i_w(s) = \{\underbrace{\frac{1}{Ls}e^{-1.5T_s s}}_{P_0(s)} + \underbrace{\left[\frac{1}{s - \Delta a}(\frac{1}{L} + \Delta b) - \frac{1}{Ls}\right]e^{-1.5T_s s}}_{\Delta P(s)}\} \cdot u_{\text{in}}(s) + \frac{d(s)}{s - \Delta a} \tag{A3}$$

where $P_0(s)$ and $\Delta P(s)$ are the nominal plant and the unmodeled dynamics, respectively. Then, we can obtain the relationship among $i_w(s)$, $u_{\text{in}}(s)$, the actual plant, and the disturbance coupled with the unmodeled system (i.e., $d'(s)$) as

$$i_w(s) = [u_{\text{in}}(s) + \underbrace{\frac{Ls}{(s - \Delta a)(e^{-1.5T_s s} + Ls \cdot \Delta P(s))}d(s)}_{d'(s)}] \cdot \underbrace{\left[\frac{1}{Ls}e^{-1.5T_s s} + \Delta P(s)\right]}_{\text{Actual Plant}}. \tag{A4}$$

According to (A4), Fig. 4 and (14) can be obtained.

References

[1] A. Reznik, M. G. Simões, A. Al-Durra, and S. M. Muyeen, "LCL filter design and performance analysis for grid-interconnected systems," *IEEE Trans. Ind. Appl.*, vol. 50, no. 2, pp. 1225–1232, Mar. 2014.

[2] D. Pan, X. Ruan, C. Bao, W. Li, and X. Wang, "Capacitor-current-feedback active damping with reduced computation delay for improving robustness of LCL-type grid-connected inverter," *IEEE Trans. Power Electron.*, vol. 29, no. 7, pp. 3414–3427, Jul. 2014.

[3] R. P. Alzola, M. Liserre, F. Blaabjerg, R. Sebastián, J. Dannehl, and F. W. Fuchs, "Analysis of the passive damping losses in LCL-filter-based grid converters," *IEEE Trans. Power Electron.*, vol. 28, no. 6, pp. 2642–2646, Jun. 2013.

[4] J. Dannehl, F. W. Fuchs, and P. B. Thogersen, "PI state space current control of grid-connected PWM converters with LCL filters," *IEEE Trans. Power Electron.*, vol. 25, no. 9, pp. 2320–2330, Sep. 2010.

[5] A. Ghoshal and V. John, "Active damping of LCL filter at low switching to resonance frequency ratio," *IEEE Trans. Ind. Electron.*, vol. 8, no. 4, pp. 574–582, Oct. 2015.

[6] B. Liu, Q. Wei, C. Zou, and S. Duan, "Stability analysis of LCL-type grid-connected inverter under single-loop inverter-side current control with capacitor voltage feedforward," *IEEE Trans. Ind. Inf.*, vol. 14, no. 2, pp. 691–702, Feb. 2018.

[7] X. Li, X. Wu, Y. Geng, X. Yuan, C. Xia, and X. Zhang, "Wide damping region for LCL-type grid-connected inverter with an improved capacitor-current-feedback method," *IEEE Trans. Power Electron.*, vol. 30, no. 9, pp. 5247–5259, Sep. 2015.

[8] W. Yao, Y. Yang, X. Zhang, F. Blaabjerg, and P. C. Loh, "Design and analysis of robust active damping for LCL filters using digital notch filters," *IEEE Trans. Power Electron.*, vol. 32, no. 3, pp. 2360–2375, Mar. 2017.

[9] D. Prez-Estévez, J. Doval-Gandoy, A. G. Yepes, Ó. Lpez, and F. Baneira, "Generalized multifrequency current controller for grid-connected converters with LCL filter," *IEEE Trans. Ind. Appl.*, vol. 54, no. 5, pp. 4537–4553, Sep. 2018.

[10] D. Prez-Estévez, J. Doval-Gandoy, A. G. Yepes, and Ó. Lpez, "Positive- and negative-sequence current controller with direct discrete-time pole placement for grid-tied converters with LCL filter," *IEEE Trans. Power Electron.*, vol. 32, no. 9, pp. 7207–7221, Sep. 2017.

[11] G. Shen, X. Zhu, J. Zhang, and D. Xu, "A new feedback method for PR current control of LCL-filter-based grid-connected inverter," *IEEE Trans. Ind. Electron.*, vol. 57, no. 6, pp. 2033–2041, Jun. 2010.

[12] Y. Ye and Y. Xiong, "UDE-based current control strategy for $LCCL$-type grid-tied inverters," *IEEE Trans. Ind. Electron.*, vol. 65, no. 5, pp. 4061–4069, May 2018.

[13] D. Pan, X. Ruan, X. Wang, F. Blaabjerg, X. Wang, and Q. Zhou, "A highly robust single-loop current control scheme for grid-connected inverter with an improved $LCCL$ filter configuration," *IEEE Trans. Power Electron.*, vol. 33, no. 10, pp. 8474–8487, Oct. 2018.

[14] D. Pan, X. Ruan, X. Wang, H. Yu, and Z. Xing, "Analysis and design of current control schemes for LCL-type grid-connected inverter based on a general mathematical model," *IEEE Trans. Power Electron.*, vol. 32, no. 6, pp. 4395–4410, Jun. 2017.

[15] J. He, Y. W. Li, D. Xu, X. Liang, B. Liang, and C. Wang, "Deadbeat weighted average current control with corrective feed-forward compensation for microgrid converters with nonstandard LCL filter," *IEEE Trans. Power Electron.*, vol. 32, no. 4, pp. 2661–2674, Apr. 2017.

[16] Y. Han, Z. Li, P. Yang, C. Wang, L. Xu, and J. M. Guerrero, "Analysis and design of improved weighted average current control strategy for LCL-type grid-connected inverters," *IEEE Trans. Energy Convers.*, vol. 32, no. 3, pp. 941–952, Sep. 2017.
[17] L. Harnefors, A. G. Yepes, A. Vidal, and J. Doval-Gandoy, "Passivity-based controller design of grid-connected VSCs for prevention of electrical resonance instability," *IEEE Trans. Ind. Electron.*, vol. 62, no. 2, pp. 702–710, Feb. 2015.
[18] J. Xu, S. Xie, Q. Qian, and B. Zhang, "Adaptive feedforward algorithm without grid impedance estimation for inverters to suppress grid current instabilities and harmonics due to grid impedance and grid voltage distortion," *IEEE Trans. Ind. Electron.*, vol. 64, no. 9, pp. 7574–7586, Sep. 2017.
[19] X. Wang, X. Ruan, S. Liu, and C. K. Tse, "Full feedforward of grid voltage for grid-connected inverter with LCL filter to suppress current distortion due to grid voltage harmonics," *IEEE Trans. Power Electron.*, vol. 25, no. 12, pp. 3119–3127, Dec. 2010.
[20] N. Alshek, M. Elkayam, and A. Kuperman, "UDE repetitive control for estimation of harmonic disturbances with time delay UDE based controller," in *Proc. IEEE Int. Conf. Sci. Electr. Eng.*, Nov. 2016, pp. 1–4.
[21] N. Alshek, S. Bronshtein, M. Elkayam, and A. Kuperman, "Modified uncertainty and disturbance estimator for enhanced periodic signals suppression," *IEEE Trans. Ind. Electron.*, vol. 66, no. 2, pp. 1246–1254, Feb. 2019.
[22] Y. Wu, Y. Ye, Q. Zhao, Y. Cao, and Y. Xiong, "Discrete-time modified UDE-based current control for LCL-type grid-tied inverters," *IEEE Trans. Ind. Electron.*, vol. 67, no. 3, pp. 2143–2154, Mar. 2020.
[23] I. Aharon, D. Shmilovitz, and A. Kuperman, "Uncertainty and disturbance estimator-based controllers design under finite control bandwidth constraint," *IEEE Trans. Ind. Electron.*, vol. 65, no. 2, pp. 1439–1449, Feb. 2018.
[24] S. Y. Gadelovits, Q. Zhong, V. Kadirkamanathan, and A. Kuperman, "Uncertainty and disturbance estimator-based controller equipped with a time-delayed filter to improve the voltage quality of inverters," *IEEE Trans. Ind. Electron.*, vol. 66, no. 1, pp. 459–469, Jan. 2019.
[25] J. Wang, J. D. Yan, L. Jiang, and J. Zou, "Delay-dependent stability of single-loop controlled grid-connected inverters with LCL filters," *IEEE Trans. Power Electron.*, vol. 31, no. 1, pp. 743–757, Jan. 2016.
[26] Q. Zhong and D. Rees, "Control of uncertain LTI systems based on an uncertainty and disturbance estimator," *J. Dyn. Syst. Meas. Control Trans.*, vol. 126, no. 4, pp. 905–910, Dec. 2004.
[27] B. Ren, Q. Zhong, and J. Dai, "Asymptotic reference tracking and disturbance rejection of UDE-based robust control," *IEEE Trans. Ind. Electron.*, vol. 64, no. 4, pp. 3166–3176, Apr. 2017.
[28] D. G. Holmes, T. A. Lipo, B. P. McGrath, and W. Y. Kong, "Optimized design of stationary frame three phase AC current regulators," *IEEE Trans. Power Electron.*, vol. 24, no. 11, pp. 2417–2426, Nov. 2009.
[29] M. Liserre, R. Teodorescu, and F. Blaabjerg, "Stability of photovoltaic and wind turbine grid-connected inverters for a large set of grid impedance values," *IEEE Trans. Power Electron.*, vol. 21, no. 1, pp. 263–272, Jan. 2006.
[30] A. G. Yepes, A. Vidal, J. Malvar, O. Lpez, and J. Doval-Gandoy, "Tuning method aimed at optimized settling time and overshoot for synchronous proportional-integral current control in electric machines," *IEEE Trans. Power Electron.*, vol. 29, no. 6, pp. 3041–3054, Jun. 2014.
[31] J. Sun, "Impedance-based stability criterion for grid-connected inverters," *IEEE Trans. Power Electron.*, vol. 26, no. 11, pp. 3075–3078, Nov. 2011.
[32] D. Pan, X. Ruan, C. Bao, W. Li, and X. Wang, "Optimized controller design for LCL-type grid-connected inverter to achieve high robustness against grid-impedance variation," *IEEE Trans. Ind. Electron.*, vol. 62, no. 3, pp. 1537–1547, Mar. 2015.

Yongkang Xiong was born in Jiujiang, China. He received the B.E. and M.E. degrees in automation and circuits and systems from the East China University of Technology, Nanchang, China, in 2012 and 2015, respectively, and the Ph.D. degree in control theory and control engineering from the Nanjing University of Aeronautics and Astronautics, Nanjing, Jiangsu, China, in 2019.

He is currently a Faculty Member with the School of Information Engineering, Nanchang University, Nanchang, China. His research interests include power electronics control and disturbance rejection control technique.

Yongqiang Ye (Senior Member, IEEE) was born in Tongxiang, China. He received the B.E. and M.E. degrees in electrical engineering from Zhejiang University, Hangzhou, China, in 1994 and 1997, respectively, and the Ph.D. degree in electrical engineering from Nanyang Technological University, Singapore, in 2004.

He was a Faculty Member with the School of Information, Zhejiang University of Finance and Economics, Hangzhou, China, for more than four years. He had also been a Postdoctoral Research Fellow with the Department of Electrical Engineering, Lakehead University, Thunder Bay, ON, Canada, the Department of Systems and Computer Engineering, Carleton University, Ottawa, ON, Canada, and the Department of Mechanical Engineering, Dalhousie University, Halifax, NS, Canada. Since 2009, he has been a Professor with the College of Automation Engineering, Nanjing University of Aeronautics and Astronautics, Nanjing, China. He is currently a Distinguished Professor at the Henan Province, affiliated with the School of Electronic and Information, Zhongyuan University of Technology, Zhengzhou, China. He has authored or coauthored one book and more than 70 journal papers. His current research interests include advanced control of power electronics and electrical machines.

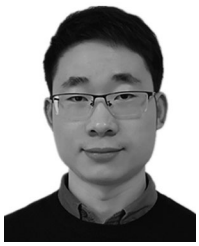

Yongfeng Cao was born in Xinyang, China. He received the B.E. degree in automation from the Central South University, Changsha, China, in 2016, and the M.E. degree in control engineering from the Nanjing University of Aeronautics and Astronautics, Nanjing, China, in 2019. He is currently working toward the Ph.D. degree in materials science and engineering with Shanghai Jiaotong University, Shanghai, China.

His current research focuses on disturbance rejection control with applications to power electronics and surgical robots.

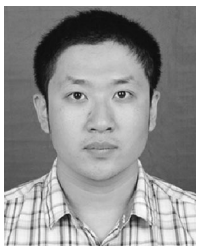

Yuheng Wu (Student Member, IEEE) was born in Jining, China. He received the B.E. and M.E. degrees in automation from the Nanjing University of Aeronautics and Astronautics, Nanjing, China, in 2015 and 2018, respectively. He is currently working toward the Ph.D. degree in electrical engineering with the Department of Electrical Engineering, University of Arkansas, Fayetteville, AR, USA.

His research interests include the field of power electronics control. Currently, his research focuses on disturbance rejection control with applications to power electronics and ac motor drivers.